Electronic Supplementary Material (ESI) for Journal of Materials Chemistry C.

Multi-Layered Graphene based Gas Sensor Platform for Volatile Organic Compounds Discrimination via Differential Intercalation

Electronic Supporting Information

Dilce Ozkendir Inanc[a], Zhi Kai Ng[b], Mehmet Baskurt[a], Berfin Keles[c], Gökay Vardar[d], Hasan Sahin[a], Siu Hon Tsang[e], Alagappan Palaniappan[f], Umit Hakan Yildiz[c,g*], EHT Teo[b,f*]

Single Layer Graphene (SLG) Growth with Epitaxial Graphene on SiC Substrate

Epitaxial graphene growth is a method based on the sublimation of the Si-atoms at high temperatures e.g., above 1300 ℃ from SiC substrate under ultra-high vacuum conditions (Fig. S1 (a)). The residual C atoms create honeycomb lattice on the SiC surface. One third of C atoms in reconstruction layers has covalent bonds to underlying Si-atoms of the topmost layers of SiC. This constructed layer has shown graphitic properties and structure. However, it strongly interacts with the substrate and leads to electronic properties which is different from an isolated graphene layer. Growth process starts at elevated temperatures that are higher than evaporation temperature of Si atoms. After evaporating Si atoms from the SiC surface, covalent bond between Si-atoms and the substrate is broken, this bond become free which constitute carbon atom to consist of sp^2 hybridization. The sublimated Si-atoms leave behind three dangling bonds of carbon atoms where in the topmost layer of the SiC these bonds form interface layer with connecting each other. Furthermore, the next graphene layer occurs in the same manner and interacts with the interface via van der Waals forces. This new graphene layer positions different with respect to two terminated faces (Fig. S1 (b)). The Si-terminated face of SiC (0001) may provide optimum AB stacking order for graphene, whereas the C-terminated face of SiC (0001) may potentially avoid ordered stacking due to dangling C bonds. This causes a weak interaction between graphene and substrate which can be explained by azimuthal asymmetry. Therefore, growth mechanism shows discrepancy with respect to Si an C terminated faces.[1]

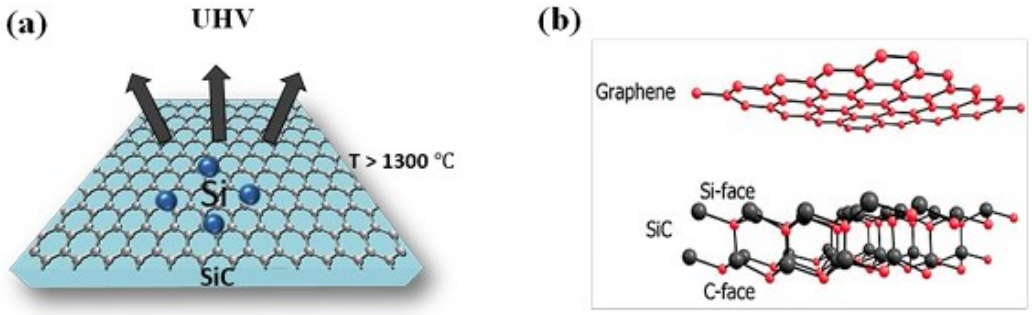

Fig. S1. Illustration of growth of epitaxial graphene under UHV condition (b) Schematics of Si and C-faces of SiC crystal

All the SLG growth experiments in this study were conducted in an ultra-high vacuum (UHV) chamber. SLG was grown in UHV chamber where base pressure is about 10^{-10} mbar. SLG growth on the SiC substrate was carried out with direct current heating method. The temperature of the sample measured by a pyrometer with a ±1 ℃ resolution. In the UHV system, utilized in this study, two different pumps were used; scroll pump and Turbo Molecular Pump (TMP). Initially, for removing the contamination such as small particles in the chamber, scroll pump was used ,which reduces the system pressure to 10^{-2} mbar. After reaching the pressure of 10^{-2} mbar, TMP is turned on to achieve a pressure in the 10^{-10} mbar range. Two types of vacuum gauges which are AUX1 (Cold Cathode) and IMG (Inverse Magnetron Gauge) were utilized. AUX1 was used to read the pressure range between 10^{-3} mbar and 10^{-9} mbar. IMG was used to read the pressure range between 10^{-3} mbar and 10^{-10} mbar. System pressure was traced by a gauge controller. All equipment and controllers for SLG growth system are shown in Fig. S2.

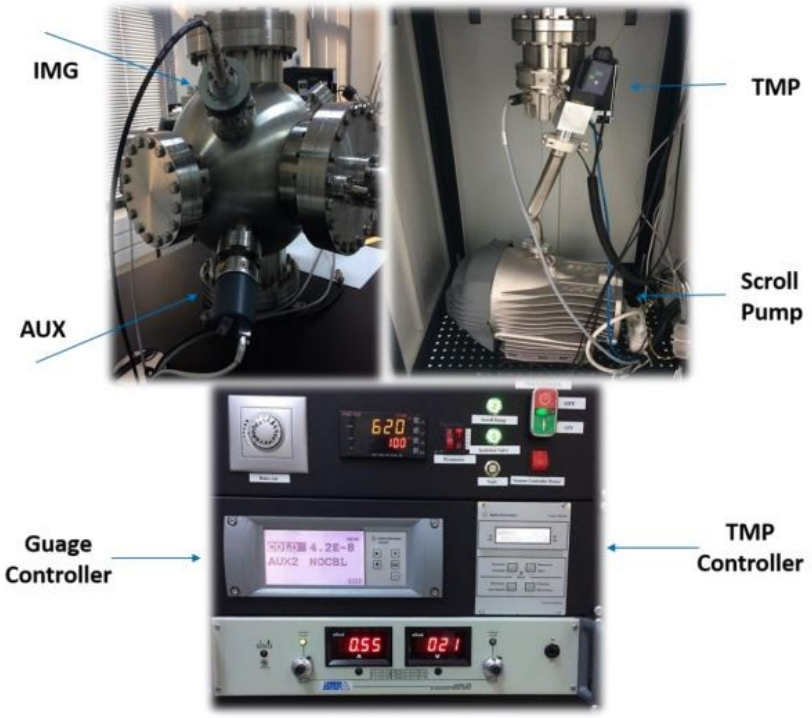

Fig. S2. SLG growth system setup

A facile and user-friendly sample stage was designed for high temperature annealing process as shown in Fig. S3 (a). Sample stage was designed with special materials to resist high temperatures in due course of growth. The lower and upper parts of the sample stage is fabricated using Alumina Ceramic (Al_2O_3) and Tantalum (Ta) (Fig. S3 (b))., respectively. These two materials have high melting points: 2072 ℃ and 3020 ℃, respectively. In addition to resisting high temperatures, Al_2O_3 act as an excellent dielectric material, which isolates Ta plates for removing any shortcut problem on the sample stage.

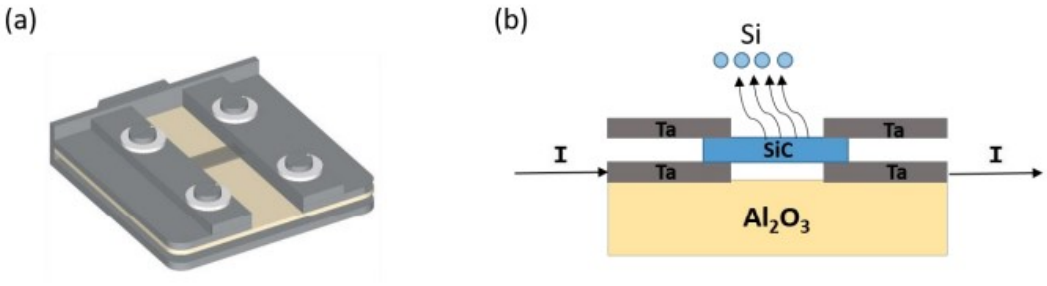

Fig. S3. (a) 3D modelling of SiC annealing sample stage for SLG growth (b) Schematic view of the sample annealing mechanism by using direct current heating method.

The growth of SLG was carried out in three steps as shown in Fig. S4 (a-c). Before the graphene growth, samples were degassed at 600 ℃ overnight. This step is necessary for thermally cleaning the organics and possible contaminations from the sample surface. For removing the native oxide layer from the sample surface, substrates were heated up to about 1050 ℃ for 5 min. To enlarge the grain boundaries of the SiC substrate, temperature was increased to 1300 ℃ for 7 min. All these procedures were carried out for every sample before the growth step. Above 1350℃ Si atoms start to evaporate from the surface and left-behind carbon atoms form graphene structure on the SiC surface. The growth was repeated as a function of temperature and time to obtain SLG (1350 ℃, 3 min).

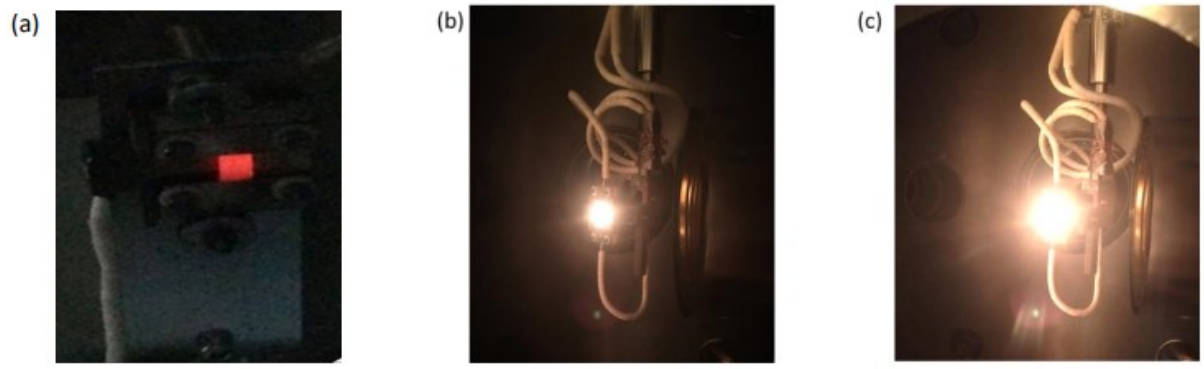

Fig. S4. SLG growth steps with different temperatures at (a) 600 ℃ (b) 1050℃ (c) 1350℃.

Bilayer Graphene (BLG) Growth with Chemical Vapor Deposition

A typical growth on Cu starts with reducing the oxides on the surface by high-temperature annealing, followed by exposure to the C precursor at the similar temperatures. The growth set-up is shown in Fig. S5. The process is started at room temperature and during all processes, Ar and H_2 were utilized to reduce the native oxide layer on the Cu foil. Here, Ar was used as an inert gas to clean the impurities that adhere onto the Cu foil and to increase the chamber pressure to unload the sample. The heating rate was always kept constant at 28°C/min from room temperature (RT) to desired growth temperature. For increasing the grain size on Cu foil, the chamber was evacuated to a pressure of 10^{-3} Torr and an annealing temperature of 990 °C for a duration of 80 min. For the growth stage, C_2H_4 decompose into C and H_2 with the help of growth temperature, H_2 flow and the catalytic activity of Cu surface facilitates

BLG growth. H_2 acts as etching reagent that controls the size and morphology of the graphene domains. After the growth was completed, the furnace is opened to the air for rapid cooling. After growth of BLG on Cu substrate, BLG were transferred on glass substrate. Microposit S1318 Photoresist (PR) was utilized as supporting layer during the graphene transfer process. The PR on the BLG graphene–Cu template was drop casted and annealed at 70 °C overnight. Iron chloride ($FeCl_3$) solution was used to etch the Cu foil. After the Cu foil was fully etched away, BLG-PR was rinsed with deionized water in order to remove any $FeCl_3$ residue. BLG-PR was transferred onto the surface of the clean glass substrate. Lastly, the PR was removed by hot acetone to leave the BLG on its own on the glass substrate.

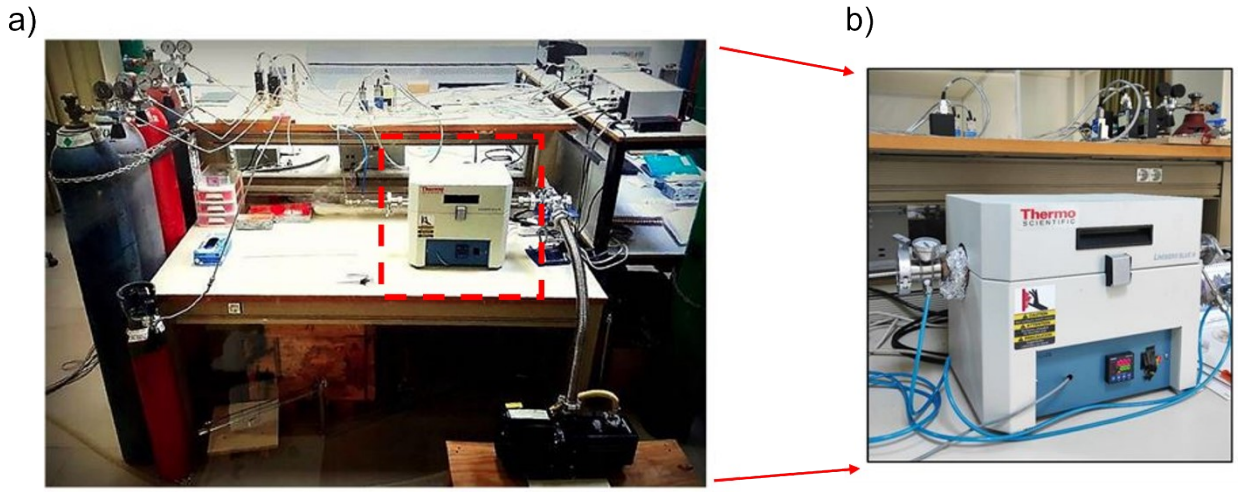

Fig. S5. a) The CVD growth set-up and b) furnace for BLG growth

Multilayer Graphene Growth

A typical CVD method for MLG growth is divided into 4 phases as shown in Fig. S6. In the ramp-up phase, after the substrate with catalyst is loaded into the chamber and flushed with inert gas, the temperature of the chamber is gradually raised in Ar and H_2 environment. For MLG synthesis, an approximate 20 °C/min increase in temperature was chosen. Subsequently, in the annealing phase, the substrate is maintained at a fixed temperature of 1000 °C in Ar/H_2 environment to remove any oxide layer on the Ni foam substrate. In the growth phase, precursor gases are injected into the chamber to initiate the growth of MLG on the Ni foam. Here, the Ni catalyzes the breakdown of the gaseous carbon precursors and the carbon dissolves into the Ni foam. After a stipulated amount of growth time, in the cooling phase, the chamber is cooled back down to room temperature. The sample is removed from the heated region for quenching to successfully synthesize MLG. The dissolved carbon will precipitate on the surface of the Ni foam during the cooling process. The Ni foam herein therefore has an additional function of providing a template for the MLG to precipitate. The photos of the devices fabricated using SLG, BLG and MLG are shown in Fig. S7.

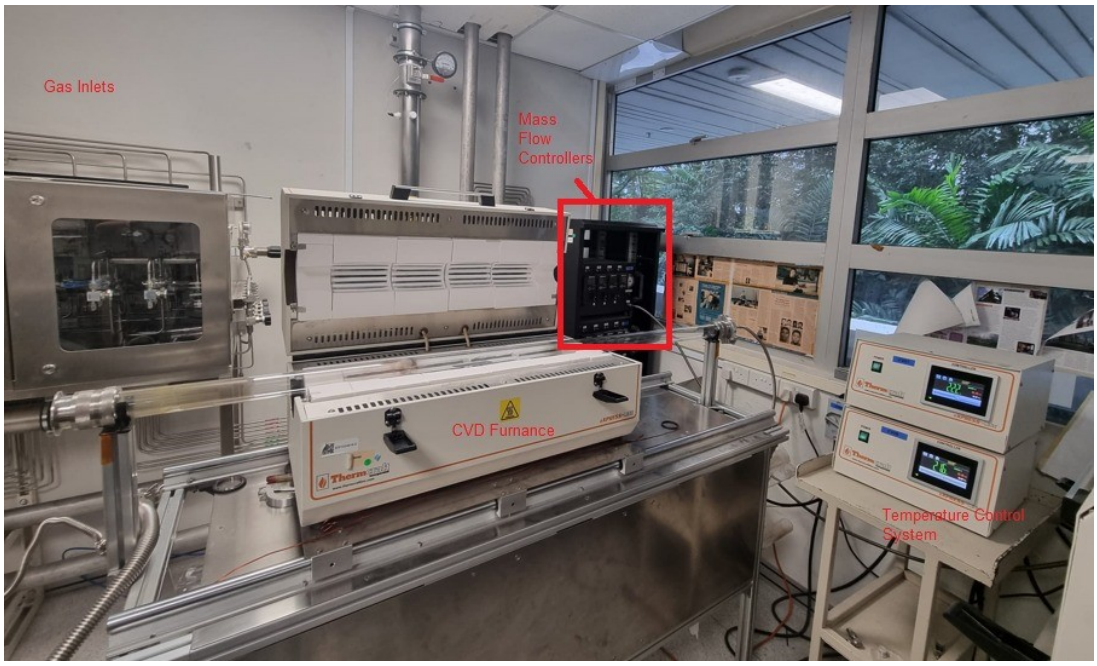

Fig. S6. CVD growth system for multilayer graphene (MLG) growth

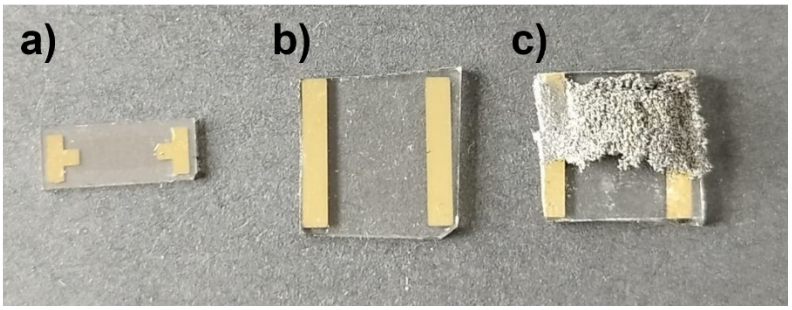

Fig. S7. a) monolayer b) bilayer and c) multilayer growth of graphene devices

DFT Calculations

DFT based calculations were performed using Vienna *ab-initio* Simulation Package (VASP) with the implemented plane-wave projector-augmented wave (PAW) potentials for investigation of interaction between MeOH/EtOH and graphene morphologies[2,4]. Perdew-Burke-Ernzerhof form of generalized gradient approximation (GGA) was used for the exchange-correlation function [5]. The van der Waals interactions were taken into consideration by the optB86b-vdw function[6,7]. The charge distribution of individual MeOH/EtOH molecules and their clusters were calculated by performing Bader analysis[8]. For a reliable approximation of the molecule-surface system, the energy cutoff of the plane-wave basis was set to 500 eV. Electronic and ionic convergence criteria were fixed at 10^{-5} and 10^{-4} eV, respectively. To avoid interactions between adjacent molecular species, at least 10 Å of vacuum spacing was set. Structural optimizations were carried until the pressures is less than 1 kB in all directions.

DFT studies were then performed to investigate the interactions between the graphene surface and a single molecule of MeOH/EtOH. During the onset of adsorption, the charge density of the graphene surface and the MeOH/EtOH molecules are modulated and redistributed. DFT calculations reveal the regions of charge modulation of graphene and individual MeOH/EtOH molecules as illustrated by cyan and green colours, respectively, in Fig. S8a. The calculated interaction energies of 297 meV and 395 meV for individual MeOH for EtOH molecule's adsorption on the graphene surface, respectively, indicates formation of electron transport channels that induces p-type doping of graphene Hence, adsorption of MeOH and EtOH reduces the sheet resistance and increases the current flowing through the graphene chemiresistors.

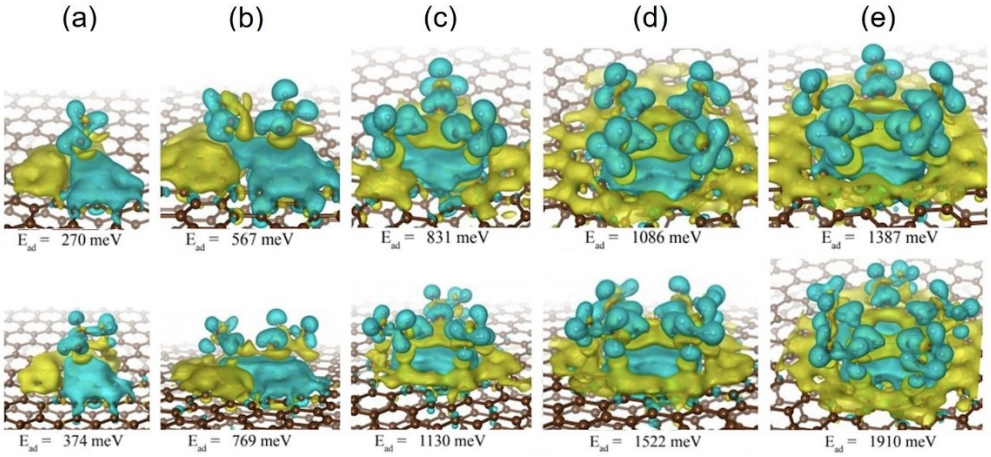

Fig. S8. Theoretical results indicating the modulations in charge density distributions of graphene (green) and MeOH/EtOH (cyan) molecules upon their adsorption on graphene surface, (a) individual molecule and (b) to (e) two to five molecules, respectively.

DFT calculations indicate that the interaction of EtOH with the graphene surface is energetically more favorable than that of MeOH regardless of the molecular cluster sizes. Fig. S8b-e shows the interaction energies of MeOH and EtOH clusters containing two to five molecules. The interaction energy increases with the cluster size, for instance, the interaction energies of pentamer, cluster containing five molecules, with the graphene surface are 1387 and 1910 meV for MeOH and EtOH clusters, respectively. The higher interaction energy ascertains that larger cluster sizes of EtOH remains on the surface of the graphene and thus inhibits their intercalation within the graphene layers. DFT analysis also concurs with previous reports based on interlayer distance that may potentially provide molecular size dependent selective intercalation of small molecules and on interaction energy between the analytes and graphene surface. In summary, DFT studies reveal that both MeOH and EtOH adsorb on to the graphene, however, MeOH is prone to intercalate within the layered graphene as compared to EtOH.

MeOH and EtOH intercalation in solution state

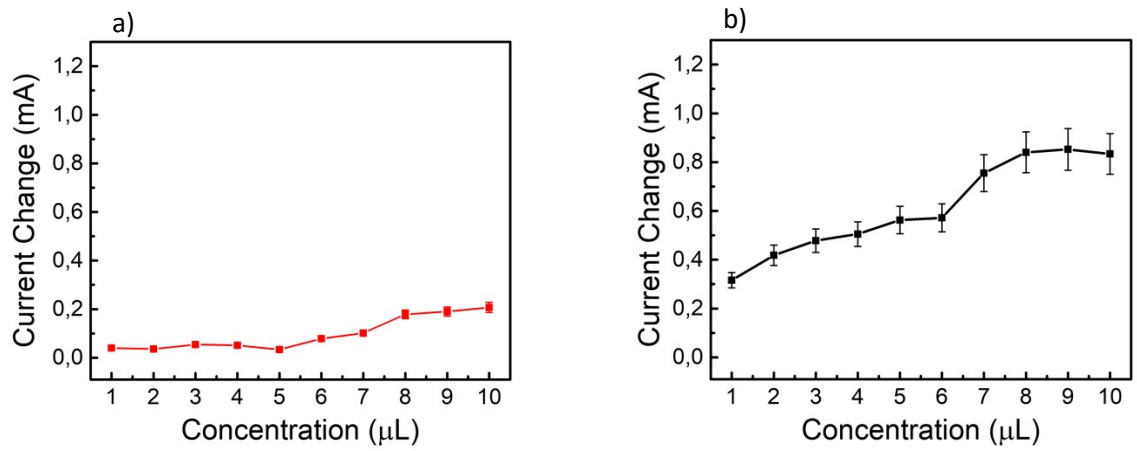

Fig. S9. a) Concentration dependent response of MLG device in the presence of a) water/EtOH and b) water/MeOH

Intercalation of water/MeOH and water/EtOH within graphene layers was monitored. As shown in Fig. S9, the larger chemiresistor were obtained upon application of water/MeOH as compared to water/EtOH mixtures. This observation ascertains that the proposed mechanism on the MeOH differential intercalation is due to its molecular structure as well as its size, which is fitting the interlayer distance of MLG.

REFERENCES

1 C. Çelebi, C. Yanik, A. G. Demirkol and I. I. Kaya, *Carbon N. Y.*, 2012, **50**, 3026–3031.

2 C. A. Zito, T. M. Perfecto and D. P. Volanti, *Sensors Actuators B Chem.*, 2017, **244**, 466–474.

3 J. H. Choi, J. Lee, M. Byeon, T. E. Hong, H. Park and C. Y. Lee, *ACS Appl. Nano Mater.*, 2020, **3**, 2257–2265.

4 C. Lv, C. Hu, J. Luo, S. Liu, Y. Qiao, Z. Zhang, J. Song, Y. Shi, J. Cai and A. Watanabe, *Nanomaterials*, 2019, **9**, 422.

5 K. Phasuksom, W. Prissanaroon-Ouajai and A. Sirivat, *RSC Adv.*, 2020, **10**, 15206–15220.

6 O. Leenaerts, B. Partoens and F. M. Peeters, *Phys. Rev. B*, 2008, **77**, 125416.

7 W. Yuan, A. Liu, L. Huang, C. Li and G. Shi, *Adv. Mater.*, 2013, **25**, 766–771.

8 F. Schedin, A. K. Geim, S. V. Morozov, E. W. Hill, P. Blake, M. I. Katsnelson and K. S. Novoselov, *Nat. Mater.*, 2007, **6**, 652–655.